Materials Characterization 134 (2017) 1–8

Contents lists available at ScienceDirect

Materials Characterization

journal homepage: www.elsevier.com/locate/matchar

# Microstructures of chemical vapor deposited high-purity tungsten achieved by two different precursors

J.Q. Shi[a], S.Y. Yao[a], F. Wang[a], X.D. Yu[a,b], H.T. Huang[c], C.W. Tan[a,b,*], Z.H. Nie[a], H.L. Ma[b], H.N. Cai[a]

[a] School of Materials Science and Engineering, Beijing Institute of Technology, Beijing 100081, China
[b] China Astronaut Research and Training Center, Beijing 100094, China
[c] Division of Reactor Engineering Technology Research, China Institute of Atomic Energy, Beijing 102413, China

ARTICLE INFO

*Keywords:*
CVD high-purity tungsten
Microstructures
Preferred orientation
Surface morphology

ABSTRACT

Chemical vapor deposited (CVD) high-purity tungsten can be manufactured as electron emitters in thermionic fuel elements. Exposed surface planes of the emitter emit electrons and affect the efficiency and load capacity of the thermionic fuel element. In order to determine the electron emission planes of the emitter, the metallurgic structures, the preferred orientation and the as-deposited surface morphology of CVD tungsten have been investigated. In this work, high-purity (over 99.99%) tungsten was achieved by two different precursors: hydrogen reduction of tungsten hexafluoride ($WF_6$) and thermolysis of tungsten hexachloride ($WCl_6$). The microstructures of CVD tungsten were characterized by metallography analysis, X-ray diffraction (XRD), electron backscattered diffraction (EBSD), and white light interference (WLI). Tungsten fabricated by hydrogen reduction of $WF_6$ and thermolysis of $WCl_6$ has ⟨100⟩-preferred columnar microstructures. However, the latter exhibits larger columnar grains and preferred ⟨100⟩ less. The preferred orientation is caused by the higher growth rate of the ⟨100⟩ orientation and competition between the ⟨100⟩ orientations of different grains. The as-deposited surface consists of tiny pyramids, with ⟨100⟩ axis and {111} side faces. In contrast to tungsten produced by hydrogen reduction of $WF_6$, the pyramid on tungsten synthesized via thermolysis of $WCl_6$ contains small {110} facets on the four edges. Therefore, tungsten made via thermolysis of $WCl_6$ is a better candidate for thermionic fuel elements, because the higher work function of {110} planes enables better output efficiency.

## 1. Introduction

Thermionic fuel elements have several advantages over solar arrays that are commonly used in spacecraft, including having a simple but stable structure with no rotating components, the possibility of miniaturization, utility in the dark, and a higher power density during constant high-power output, among others [1,2]. The cathode (electron emitter) in the thermionic energy converter serves as the “heart” of the thermionic fuel element (Fig. 1 is a diagram). Heated by encapsulated nuclear fuels, the emitter operates at a high ambient temperature of approximately 1500 °C throughout the service period.

Chemical vapor deposited tungsten has a combination of excellent properties, namely high-purity, high density, the capability of forming preferred orientations and heterotypic shaping, which enables the use of CVD tungsten in vital electronic and nuclear applications [3]. CVD tungsten can be used to manufacture electron tubes, field emitting tips in electron microscopes, and electron emitters in thermionic fuel elements [4–6]. Work function affects the electron emission properties significantly, and different applications have different work function requirements—a higher working current requires a lower work function, making electrons prone to emission, whereas a higher working voltage requires a higher work function, preventing electron emission [7]. The influence of the work function is even notable for CVD tungsten used as the electron emitter in a thermionic fuel element. An emitter with higher work function enables the thermionic fuel element to work at a higher voltage and increase its efficiency and load capacity [7–9]. Although tungsten has a relatively high work function, work functions of different crystal planes can vary widely—{110} planes have the highest work function, followed by {112} planes, {100} planes, and {111} planes with the lowest work function (see Table 1) [7,9,10].

Thus, the surface electron emission planes, determined by the preferred orientation and the as-deposited surface morphology of CVD tungsten, affect the work function of the electron emitter remarkably.

* Corresponding author at: School of Materials Science and Engineering, Beijing Institute of Technology, Beijing 100081, China.
*E-mail address:* tanchengwen@bit.edu.cn (C.W. Tan).

http://dx.doi.org/10.1016/j.matchar.2017.10.007
Received 19 July 2017; Received in revised form 25 August 2017; Accepted 2 October 2017
Available online 04 October 2017
1044-5803/ 

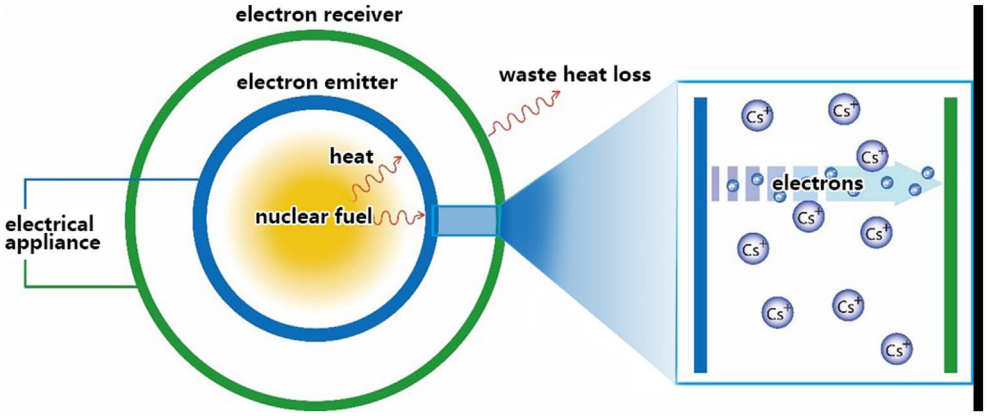


**Fig. 1.** A diagram of thermionic fuel element.

**Table 1**
Work functions of different tungsten planes.

| Crystal plane | {110} | {112} | {100} | {111} |
|---|---|---|---|---|
| Work function (eV) | 5.40 | 4.80 | 4.54 | 4.37 |

Previous studies primarily focused on CVD methods to fabricate tungsten, including hydrogen reduction of $WF_6$, hydrogen reduction of $WCl_6$ and thermolysis of $WCl_6$, along with the microstructures of the resultant tungsten [11–14]. In order to have a better understanding of the electron emission planes of the emitter and further optimize the efficiency and load capacity of the thermionic fuel element, detailed investigations into the causes of the preferred orientation and the as-deposited surface morphology of CVD tungsten are required.

Here, we studied the metallurgic structures, preferred orientation, and as-deposited surface morphology of CVD high-purity (over 99.99%) tungsten fabricated by hydrogen reduction of $WF_6$ and thermolysis of $WCl_6$. The metallurgic structures were studied by optical microscope. The preferred orientation was characterized by X-ray diffraction (XRD) and electron backscattered diffraction (EBSD). The as-deposited surface morphology was investigated using a scanning electron microscope (SEM) and white light interference (WLI). The microstructural difference caused by two different CVD precursors, the causes of the preferred ⟨100⟩ orientation, and the formation of as-deposited surface morphology are also discussed in detail.

## 2. Experimental

In this work, high-purity tungsten was deposited on polycrystalline Mo substrates by two different CVD precursors, hydrogen reduction of $WF_6$ (WF tungsten) and thermolysis of $WCl_6$ (WCl tungsten). WF tungsten was made in a vertically positioned cold-wall stainless steel chemical vapor deposition reactor, operating at approximately 550 °C and 101 kPa (1 atm), whereas WCl tungsten was made in a vertically positioned cold-wall stainless steel chemical vapor deposition reactor, operating at approximately 1540 °C and a low pressure of approximately 16 Pa.

Purity measurements of tungsten were performed using glow discharge mass spectrometry (GDMS, Thermo Fisher Scientific VG9000) and instrument gas analysis (IGA, EMGA-621W Hydrogen Analyzer, LECO ONH 836 Oxygen and Nitrogen Analyzer, and LECO CS-844 Carbon and Sulfur Analyzer). The results show that both WF tungsten and WCl tungsten are > 99.99% pure, and the impurities are C, H, O, F (WF tungsten), and Cl (WCl tungsten).

The deposited WF tungsten was 1 mm thick. The thickness of the deposited WCl tungsten was 1.5 mm. Samples were cut using an electro-discharge wire cutting machine and then milled to eliminate cutting marks. Samples for metallography observation (optical microscope, Olympus BX51M) were polished to a mirror-like, bright surface using 0.5 μm diamond polishing paste. Then, samples were submerged in an etchant ($H_2O$: NaOH: $K_3Fe(CN)_6$ = 8 ml:1 g:1 g) for 25 s to expose the metallography [15]. Samples for XRD (Rigaku SmartLab high-resolution XRD, $CuK_{\alpha 1}$, working at 40 kV and 180 mA) were ground to a fine finish by abrasive paper. X-ray pole figures were measured by a 5 × 5° collection grid. Data analysis was performed using Matlab MTEX toolbox. Samples for EBSD (JEOL JSM-7001F SEM, with Orientation Imaging Microscopy Analysis developed by EDAX) were further polished using a solution of 0.05 μm $SiO_2$ and $H_2O_2$. Samples for as-deposited surface morphology observation (FEI Quanta 650 SEM with Oxford Aztec EBSD system, and ZYGO Newview WLI) were ultrasonically cleaned in deionized water and ethanol without any milling or polishing. To further understand the orientations of the facets on the as-deposited surface, Kikuchi patterns generated by electron diffraction were captured and automatically analyzed by Oxford Aztec.

## 3. Results and Discussions

### 3.1. Metallography Observation

The metallurgic structures of WF tungsten and WCl tungsten are shown in Fig. 2. Both WF tungsten and WCl tungsten exhibit obvious columnar grain structures. They appear to have three growth stages (shown in Fig. 2): (1) nucleation and growth of primitive nearly equiaxed grain with random orientations (shown in Fig. 3); (2) formation of premature small columnar grains, which is a transitional stage; and (3) stable growth of mature large columnar grains with a preferred orientation normal to the substrate. In this stage, a few columnar grains as high as the thickness of the CVD tungsten may exist, but most columnar grains are stopped by fine grains nucleated at the grain boundaries nearby.

Average grain sizes of WF and WCl tungsten in different stages are shown in Table 2. For WF tungsten, the height-to-width ratio of columnar grains is 6 to 15. For WCl tungsten, the height-to-width ratio is 1.5 to 9.

According to research on CVD nucleation and growth processes conducted by R.D. Gretz and J.P. Hirth [16], the nucleation rate of tungsten CVD process, $J$, equals

$$J = \frac{\alpha \mathrm{aPq}\, ln\, \mathrm{S}\, sin\, \theta}{2\sqrt{2\pi \mathrm{m} f(\theta)\gamma}} \times exp\left(\frac{\Delta G^*_{des} - \Delta G^*_{dif}}{\mathrm{kT}}\right) \times exp\left(\frac{-16\pi\gamma^3\Omega^2 f(\theta)}{\mathrm{k}^3\mathrm{T}^3(ln\,\mathrm{S})^2}\right), \quad (1)$$

where $\alpha$ is the condensation coefficient, a is the molecular surface spacing, P is the vapor pressure, q is the concentration of substrate sites, S is the supersaturation (ratio of deposition pressure to equilibrium pressure, $P_d/P_e$) of the CVD system, $\theta$ is the contact angle, m is the molecular mass, $f(\theta)$ is the ratio of the nucleus volume to the volume of a sphere of the same curvature (a function of $\theta$), $\gamma$ is the surface energy,